MICROPLANE MODEL M4 FOR CONCRETE. II: ALGORITHM AND CALIBRATION

By Ferhun C. Caner[1] and Zdeněk P. Bažant,[2] Fellow, ASCE

ABSTRACT: This paper represents Part II of a two-part study in which a new improved version of the microplane constitutive model for damage-plastic behavior of concrete in 3D is developed. In Part II, an explicit numerical algorithm for model M4 is formulated, the material parameters of model M4 are calibrated by optimum fitting of the basic test data available in the literature, and the model is verified by comparisons with these data. The data in which strain localization must have occurred are delocalized, and the size effect is filtered out from the data where necessary. Although model M4 contains many material parameters, all but four have fixed values for all types of concretes. Thus the user needs to adjust only four free material parameters to the data for a given concrete, for which a simple sequential identification procedure is developed. If the user's data consist only of the standard compression strength and the strain at uniaxial stress peak, the adjustment is explicit and immediate. Good agreement with an unusually broad range of material test data is achieved.

INTRODUCTION

Part I of this study has led to the development of a new improved version of the microplane constitutive model for the nonlinear triaxial constitutive model for damage-plastic behavior of concrete, including postpeak softening. This model, labeled M4, is the fourth generation of microplane models formulated at Northwestern University. In this Part II, the numerical algorithm for model M4 is constructed, the material parameters of model M4 are calibrated by optimum fitting of the basic test data available in the literature, and the model is verified by comparisons with these data. All the definitions and notations from Part I are retained.

EXPLICIT NUMERICAL ALGORITHM

At each integration point of each finite element in each loading step of an explicit finite-element program in which the strain values and their increments are given, the material subroutine must deliver the corresponding stresses. These stresses may then be used in the integration over each element to get the internal force vector of the element, which may then be assembled to yield the internal force vector of the structure.

The values of $\vec{n}$, $\vec{m}$, $\vec{l}$, $N_{ij} = n_i n_j$, $M_{ij} = \text{sym}\ n_i m_j$, and $L_{ij} = \text{sym}\ n_i l_j$ for each microplane are generated and stored before structural analysis. The algorithm for the material subroutine is given below. The algorithm for the driver to this subroutine, used for material data fitting, is given in Appendix I.

1. The (macro) strains ε_{ij}, their increments $\Delta\varepsilon_{ij}$, the microplane stresses σ_N^{pre}, σ_L^{pre}, and σ_M^{pre} obtained in the previous load step or iteration for each microplane, and σ_V^{pre}, which is the same for all microplanes, are given.
2. Apply the kinematic constraint to get the microplane strain components $\Delta\varepsilon_N = N_{ij}\Delta\varepsilon_{ij}$; $\Delta\varepsilon_V = \Delta\varepsilon_{kk}/3$; $\Delta\varepsilon_D = \Delta\varepsilon_N - \Delta\varepsilon_V$; $\Delta\varepsilon_L = L_{ij}\Delta\varepsilon_{ij}$; and $\Delta\varepsilon_M = M_{ij}\Delta\varepsilon_{ij}$.
3. Check the loading criterion in (22) of Part I (Bažant et al. 2000c) to decide the value of the incremental elastic modulus for each microplane strain component.
4. Compute $\sigma_V^e = \sigma_V^{\text{pre}} + \max(E_V, dF_V^-/d\varepsilon_V)\Delta\varepsilon_V$ and the boundary values $\sigma_V^{b-} = F_V^-(-\varepsilon_V)$ and $\sigma_V^{b+} = F_V^+(\varepsilon_V)$; set
$$\sigma_V^* = \min[\max(\sigma_V^{b-}, \sigma_V^e), \sigma_V^{b+}] \tag{1}$$
5. Compute $\sigma_D^e = \sigma_D^{\text{pre}} + E_D\Delta\varepsilon_D$ and the boundary values $\sigma_D^{b-} = F_D^-(\varepsilon_D)$ and also $\sigma_D^{b+} = F_D^+(\varepsilon_D)$; calculate
$$\sigma_D = \min[\max(\sigma_D^{b-}, \sigma_D^e), \sigma_D^{b+}] \tag{2}$$
6. For each microplane, compute $\sigma_N = \sigma_V^* + \sigma_D$, and also σ_N at the boundary as $\sigma_N^b = F_N(\varepsilon_N)$. But, to prevent violating the normal tensile softening and crack-closing boundaries, set
$$\sigma_N = \min(\sigma_N, \sigma_N^b) \tag{3a}$$
and if
$$\varepsilon_N > 0 \quad \text{and} \quad \sigma_N < 0 \quad \text{reset} \quad \sigma_N = 0 \tag{3b}$$
7. Recalculate σ_V as the average of the microplane normal stress σ_N over the surface of the unit hemisphere. But to prevent this value from exceeding the volumetric stress calculated in item 4 as σ_V^*, set
$$\sigma_V = \min\left(\int_\Omega \sigma_N\, d\Omega/2\pi, \sigma_V^*\right) \tag{4}$$
8. Recalculate $\sigma_D = \sigma_N - \sigma_V$ for each microplane.
9. Calculate the shear stress at the boundary as $\sigma_T^b = F_T(\sigma_N)$ and the elastic shear stresses as $\sigma_L^e = \sigma_L^{\text{pre}} + E_T\Delta\varepsilon_L$ and $\sigma_M^e = \sigma_M^{\text{pre}} + E_T\Delta\varepsilon_M$. For the friction boundary, now use one alternative: *Alt-I* (50% faster, less accurate)—Calculate the shear stresses in $\vec{l}$ and $\vec{m}$ directions respectively, as $\sigma_L = \text{Sign}(\sigma_L^e)\min(|\sigma_T^b|, |\sigma_L^e|)$ and $\sigma_M = \text{Sign}(\sigma_M^e)\min(|\sigma_T^b|, |\sigma_M^e|)$; *Alt-II* (slower, consistent, more accurate)—Calculate the resultant of the elastic shear stresses as $\sigma_T^{eR} = \sqrt{(\sigma_L^e)^2 + (\sigma_M^e)^2}$, and determine the unit vector in the direction of the resultant, $\vec{R} = (\sigma_L^e, \sigma_M^e)/\sigma_T^{eR}$. Compute $\sigma_T^R = \min(\sigma_T^b, \sigma_T^{eR})$ (note that $\sigma_T^b > 0$). Obviously, vector $(\sigma_L, \sigma_M) = \sigma_T^R\vec{R}$.
10. Update microplane stresses σ_N, σ_M, and σ_L for each microplane and update σ_V only once (it is the same for all microplanes).
11. Compute the components of the (macro) stress tensor by numerical integration over a unit hemisphere according to (12) of Part I (Bažant et al. 2000c) and supply it to the driver (a finite-element program, or main program for material response).

The method of return to the normal, volumetric, and deviatoric boundaries is a special case, on the microplane compo-

[1]Grad. Res. Asst., Dept. of Civ. Engrg., Northwestern Univ., Evanston, IL 60208-3109.

[2]Walter P. Murphy Prof. of Civ. Engrg. and Mat. Sci., Northwestern Univ., Evanston, IL. E-mail: z_bazant@northwestern.edu

Note. Associate Editor: Gilles Pijaudier-Cabot. Discussion open until February 1, 2001. Separate discussions should be submitted for the individual papers in this symposium. To extend the closing date one month, a written request must be filed with the ASCE Manager of Journals. The manuscript for this paper was submitted for review and possible publication on March 2, 1999. This paper is part of the ***Journal of Engineering Mechanics***, Vol. 126, No. 9, September, 2000. ©ASCE, ISSN 0733-9399/00/0009-0954–0961/$8.00 + $.50 per page. Paper No. 20388.

nent level, of the widely used radial return algorithm. But the return to the friction boundary is not a radial return in the stress component space (a radial return is not possible because, after some initial inelastic deformation, the frictional yield surface for the microplane passes through the origin).

In simulating the response of a specimen that deforms approximately homogeneously, a special case of this algorithm with an iterative driver (main program) is used.

OPTIMIZATION OF MODEL PARAMETERS TO FIT TEST DATA

The fixed parameters are denoted as c_i ($i = 1, \ldots, 17$). By optimizing the fits of test data, their values have been determined as

$$c_1 = 0.62; \quad c_2 = 2.76; \quad c_3 = 4.00; \quad c_4 = 70; \quad c_5 = 2.50 \qquad (5a\text{–}e)$$

$$c_6 = 1.30; \quad c_7 = 50; \quad c_8 = 8.00; \quad c_9 = 1.30; \quad c_{10} = 0.73 \qquad (5f\text{–}j)$$

$$c_{11} = 0.2; \quad c_{12} = 7{,}000; \quad c_{13} = 0.20; \quad c_{14} = 0.5 \qquad (5k\text{–}n)$$

$$c_{15} = 0.02; \quad c_{16} = 0.01; \quad c_{17} = 0.4 \qquad (5o\text{–}q)$$

The typical values of the adjustable parameters, denoted as k_i ($i = 1, \ldots, 4$), have been found to be

$$k_1 = 1.5 \times 10^{-4}; \quad k_2 = 500; \quad k_3 = 15; \quad k_4 = 150 \qquad (6a\text{–}d)$$

Poisson's ratio can be taken as $\nu = 0.18$ for most types of concrete. For various concretes the adjustable parameters may vary approximately within the following ranges: $0.8 \times 10^{-4} \le k_1 \le 2.5 \times 10^{-4}$; $100 \le k_2 \le 1{,}000$; $5 \le k_3 \le 15$; and $30 \le k_4 \le 200$.

A change in the E-modulus causes a vertical scaling transformation (affinity transformation) of all the response stress-strain curves. Upon changing the modulus from E to some other value E', all the stresses are multiplied by the ratio E'/E at no change of strains (which is a vertical affinity transformation with respect to the strain axis). A change in parameter k_1 causes radial scaling (polar affinity transformation) of any stress-strain curve with respect to the origin. If this parameter is changed from k_1 to some other value k_1', all the stresses and strains are multiplied by the ratio k_1'/k_1 (Bažant et al. 1996b). If a vertical scaling by factor E'/E (obtained by replacing E by E') is combined with a radial scaling by factor $k_1 = E/E'$, the result is a horizontal scaling by factor k_1 of all the response curves (horizontal affinity transformation with respect to the stress axis). Carrying out scaling transformations has shown in which manner E and k_1 must appear in the foregoing equations so as not to affect the shapes of the response curves. The shapes are controlled by the remaining parameters $k_2, \ldots, k_4, c_1, \ldots, c_{17}$.

The value $E = 25$ GPa together with the values $k_1 = 2.45 \times 10^{-4}$, $k_2 = 110$, $k_3 = 12$, and $k_4 = 38$ of adjustable parameters yields the uniaxial compression strength $f_c' = 46$ MPa and the axial normal strain at peak stress $\varepsilon_p = 0.0036$, as determined by simulation of the uniaxial compression test. If one needs a microplane model that yields the uniaxial compressive strength f_c^* and the corresponding strain at peak ε_p^*, it suffices to replace the reference values of parameters k_1 and E by the values

$$k_1^* = k_1 \frac{\varepsilon_p^*}{\varepsilon_p}; \quad E^* = E \frac{f_c^*}{f_c'} \frac{\varepsilon_p}{\varepsilon_p^*} \qquad (7a,b)$$

The aforementioned reference values of material parameters yield the following ratios characterizing the behavior of concrete:

$$\frac{f_t'}{f_c'} = 0.068; \quad \frac{f_{bc}'}{f_c'} = 1.135; \quad \frac{f_c^s}{f_c'} = 0.076 \qquad (8a\text{–}c)$$

$$\frac{\sigma_r}{f_c'} = 0; \quad \frac{\tau_r}{f_c^s} = 0.097 \qquad (8d,e)$$

where f_c' = uniaxial compressive strength; f_t' = uniaxial tensile strength; f_{bc}' = biaxial compressive strength; f_c^s = pure shear strength; σ_r = residual stress for very large uniaxial compressive strain; and τ_r = residual stress for very large shear strain (at $\sigma_V = 0$). The transformations according to (7) do not change these ratios, which can be changed by adjusting material parameters other than E and k_1.

Before the fitting of a set of test data, it is necessary to decide whether the deformation of the specimen was almost uniform or whether it localized. If the latter were the case, the data need to be corrected or delocalized. For tensile tests of large specimens, it is further necessary to filter out the size effect from the test data. Both corrections to the test data may be carried out according to the approximate procedure described in Bažant et al. (1996a).

The model parameters have been optimized so as to make the responses very close to the typical test data that exist, especially those from triaxial tests at various confining pressures. In the optimization, the same values have been used for most of the parameters. The fixed parameters are those for which the optimization yielded nearly the same values for different concretes. The user who needs to optimize the model for a particular concrete needs to adjust only the free parameters.

Striving to optimize the fits of extensive test data, one need not vary all four free parameters simultaneously. Starting with the given values of E and ν and assuming the reference values for all the other parameters, one can proceed in the following three stages:

1. Optimize parameters k_3 and k_4 of the volumetric boundary by optimally fitting the hydrostatic compression test data alone.
2. Determine the radial scaling coefficient k_1, either simply from the strain at peak uniaxial compressive stress, or, better, by optimally fitting the entire stress-strain curve for unconfined (uniaxial) compression.
3. Determine the asymptotic value of the frictional boundary k_2 by optimally fitting triaxial compression test data with confinement strong enough to make concrete response almost plastic (i.e., without significant postpeak softening).

Furthermore, by varying c_{17} (with k_1), the postpeak slope in uniaxial compression can be changed. Similarly, the postpeak slope in unconfined tension can be altered by changing c_3. Such optimizations, however, are not so easy since other types of response are also affected.

Calibrating model M4 for a given concrete according to steps 1 to 3 necessitates test data for only uniaxial compression, triaxial compression at various pressures, and hydrostatic compression. In most practical applications, confining pressures are not high enough to cause pore collapse in concrete, which means that the compressive volumetric boundary does not matter. Then step 1 can be omitted and parameters k_3 and k_4 can be assigned their aforementioned reference values, which means that the user needs to adjust only k_1 and k_2 according to steps 2 and 3—an almost trivial task. Often even the triaxial test data are unavailable, and in that case the aforementioned reference value of k_2 is used, and step 3 is omitted.

The main role of each fixed parameter may be briefly summed up as follows:

- c_1—controls peak stress magnitude under uniaxial (unconfined) tension
- c_2—controls roundness of peak in uniaxial tension
- c_3—controls steepness of postpeak descent in uniaxial tension
- c_4—same as c_3, but for tensile volumetric strain
- c_5—controls volumetric expansion in compressive uniaxial stress test
- c_6—controls roundness of peak of volumetric expansion in compressive uniaxial stress test
- c_7—controls steepness of postpeak descent in compressive uniaxial stress test
- c_8—controls peak magnitude in compressive uniaxial stress test
- c_9—controls peak roundness in compressive uniaxial stress test
- c_{10}—controls pressure effect in standard triaxial tests
- c_{11}—sets magnitude of initial cohesion in frictional response
- c_{12}—controls decrease of cohesion with increasing volume expansion (frictional cohesion damage)
- c_{13}, c_{14}—control lateral contraction in uniaxial tension
- c_{15}, c_{16}—control effects of volumetric strain and volumetric stress on unloading slope E_V^U in hydrostatic compression tests
- c_{17}—controls degree of damage manifested in unloading slopes

Adjustment of the postpeak descending slope of the stress-strain curves can be achieved according to the series coupling model for localization, which may be applied directly to the stress-strain boundaries at the microplane level [in the manner of Eq. (1) of Bažant and Xiang et al. (1996b) and also of the localization approach of Cofer and Kohut (1994)].

The volume dilatancy due to shear or deviatoric strains, and the pressure developed when volume change during shear strain is restricted, are controlled by the degree of asymmetry of the deviatoric and normal boundaries, mainly by the ratios c_8/c_5, c_2/c_5, and c_9/c_6 and the value of c_{17}. To understand this volume dilatancy, note that when pure shear strain is applied on a certain plane, the material is compressed in one direction with a 45° inclination to the shear plane and also extended in a direction with the opposite 45° degree inclination. If the normal and deviatoric boundaries were symmetric, the resultant (normal to the shear plane) of the normal forces in these two directions would vanish, but because the tensile boundaries are lower than the compressive ones, the resultant of these forces is nonzero and compressive.

Are there too many parameters? Skeptical purists will doubtless decry that there are, as they have always done. For the user, however, the important points are that, depending on the pressure range, there are in model M4 only two or four free parameters, and they can be identified sequentially. As for the remaining, fixed parameters, the user need not bother. For the purist, the point to realize is that in a quarter century of intense researches, nobody has yet come up with an acceptable general model with fewer than 15 parameters (and these models have not been as comprehensive as M4, by far). The problem is that concrete is more complex than most other materials. The graphical characterization of its nonlinear triaxial behavior necessitates the curves for at least seven different characteristic types of responses, and the curve-fitting of each of these responses necessitates no fewer than three or four parameters. Looking at it from the viewpoint of microstructure, to characterize its geometry at several scales, the mechanical properties of all the constituents, their mutual bonding, defects, and pores, one needs at least 25 parameters.

CALIBRATION AND COMPARISON WITH TEST DATA

The model has been calibrated by fitting two groups of test data: (1) the typical data from the literature (Balmer 1949; Bresler and Pister 1958; Sinha et al. 1964; Kupfer et al. 1969; Launay and Gachon 1971; Green and Swanson 1973; Petersson 1981; Reinhardt and Cornelissen 1984; van Mier 1984, 1986), obtained on different concretes, and (2) further comprehensive test data from the Waterways Experiment Station (WES), reported in Bažant et al. (1996a), which were obtained for one and the same concrete by one and the same group of researchers. Most of these data were previously used to calibrate model M3 as well. The first group of data is chosen to determine the range of parameters and, more importantly, to differentiate the free parameters from the fixed ones. The second group of data has been more difficult to fit because it deals with diverse atypical triaxial loadings, but reasonable approximations are nevertheless achieved. Significant improvements over the previous version M3 can be seen by comparisons with the fits of the same data sets in Bažant et al. (1996a) and Bažant and Prat (1988b).

The uniaxial (unconfined) compression test data of van Mier (1986) are fit very closely by the model, as seen in Fig. 1(a). The curve of the model is also shown with an enlarged strain range to demonstrate that at large enough compressive strain the axial stress does get reduced to zero, unlike with previous models. To achieve this reduction, simultaneous tensile normal, volumetric, and deviatoric boundaries have been necessary.

Fig. 2(a) depicts similar test data obtained recently at WES, and their fit is seen to be also successful. The smooth rounded peaks in these figures are achieved by virtue of the newly introduced horizontal (yield) boundaries, equivalent to plastic yield limits. In contrast to the previous versions, the descending slope of the postpeak softening response can now be controlled independently of the curvature at stress peak, which made possible a good fit in Fig. 1(a).

Another response that has been difficult to simulate is the dependence of the volume expansion on the axial stress measured in uniaxial (unconfined) tests. Fig. 1(b) depicts the test data by van Mier (1984) and the response predicted by the model. A better agreement with the data is attained than with the previous microplane models, except for the initial and final phases of expansion.

Fitting the triaxial compression test data has been difficult, for two reasons. First, for the same concrete, there are different types of tests to fit simultaneously, with the same set of parameters. Second, the behavior in the uniaxial (unconfined) compression, which is a limiting special case of the triaxial tests for vanishing confining pressure, is completely different from the behavior at high confining pressures. Figs. 1(c) and 2(b) show that the present new version of the model can nevertheless adequately describe these data, as well as further data for different types of concrete.

The biaxial failure envelope tested by Kupfer et al. (1969) is also simulated quite closely by the present model [Fig. 1(d)].

Fig. 3(a) shows the triaxial failure envelope in the octahedral plane (π-plane) measured by Launay and Gachon (1971) on cubical specimens in true triaxial tests with a nonproportional loading sequence shown in the figure. Note that model M4 correctly predicts that for low hydrostatic pressure (curve for $\sigma_V = -f_c'/3$, with $\sigma_0 = -f_c'$), the envelope is a rounded triangle (a hexagon with three squashed vertices), while for increasing pressures it is becoming more and more circular (curve for $\sigma_V = -(11/3)\,f_c'$, with $\sigma_0 = -6.7\,f_c'$). Such behavior is logical because a circular shape corresponds to a horizontal Mohr failure envelope, which characterizes plasticity and is apparently approached for extremely high pressures, and a nearly triangular shape (a squashed hexagon) corre-

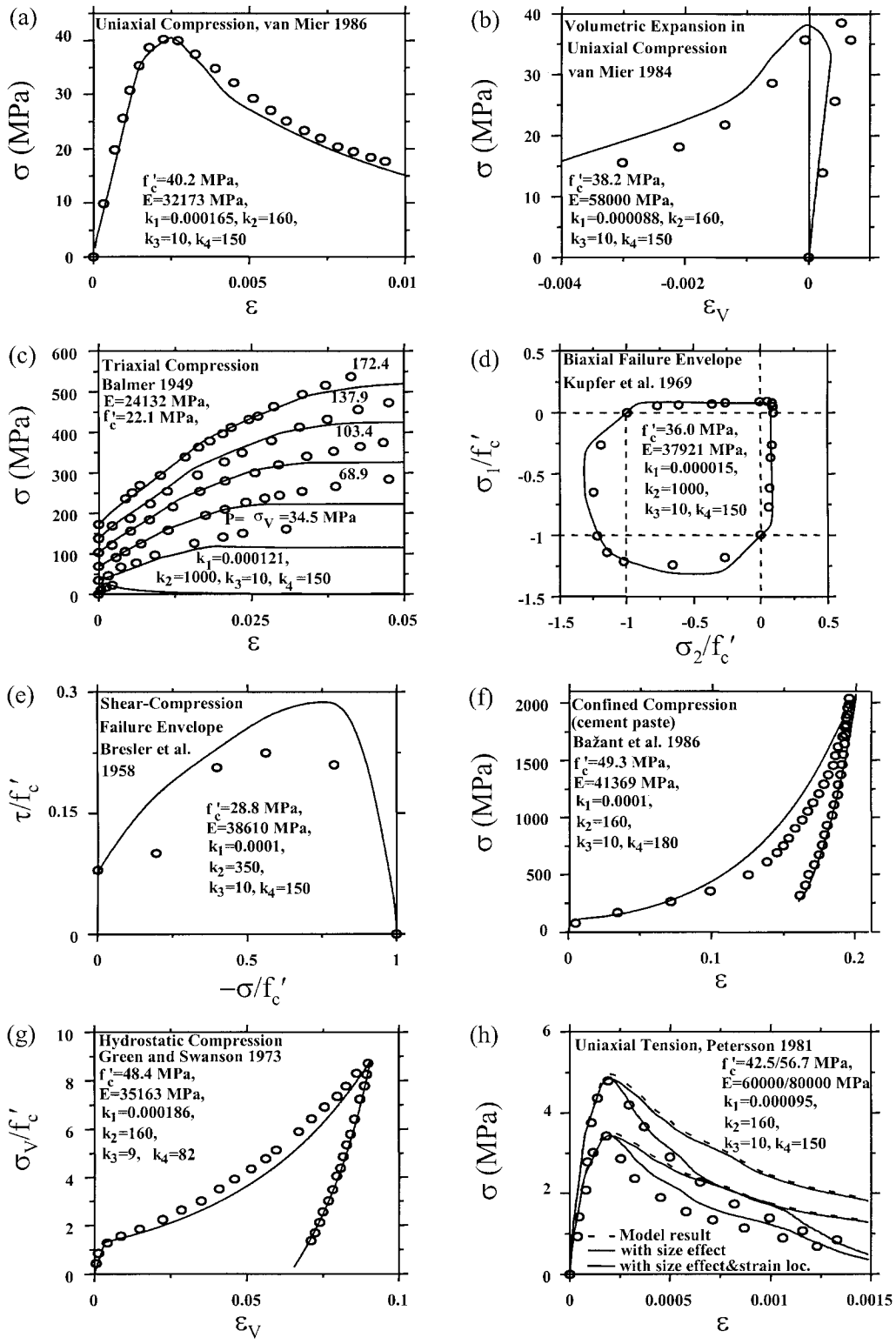

FIG. 1. Basic Test Data from Literature and Their Optimized Fits with Model M4

sponds to a sharply inclined Mohr failure envelope, which characterizes a frictional material failing in tension and having a much higher uniaxial compression strength. Note that this kind of plot is very sensitive to the testing method, and different authors give very different results (e.g., Aschl et al. 1976).

Figs. 2(c and d) demonstrate a good prediction for certain special biaxial loading paths tested at WES, for which the lateral-to-axial strain ratio has been kept fixed as -0.2. This means that a tensile strain prescribed in lateral direction, equal to 20% of the axial compressive strain, is enforced in the lateral direction.

Figs. 2(e and f) depict the fits of the experimental data for confined uniaxial compression strain loading followed by lateral strain unloading. In this very special type of test, the simulated response is very close to the data.

The shear-compression failure envelope measured by Bresler and Pister (1958) has been successfully represented by the model, as shown in Fig. 1(e). This is an improvement over the previous version M3.

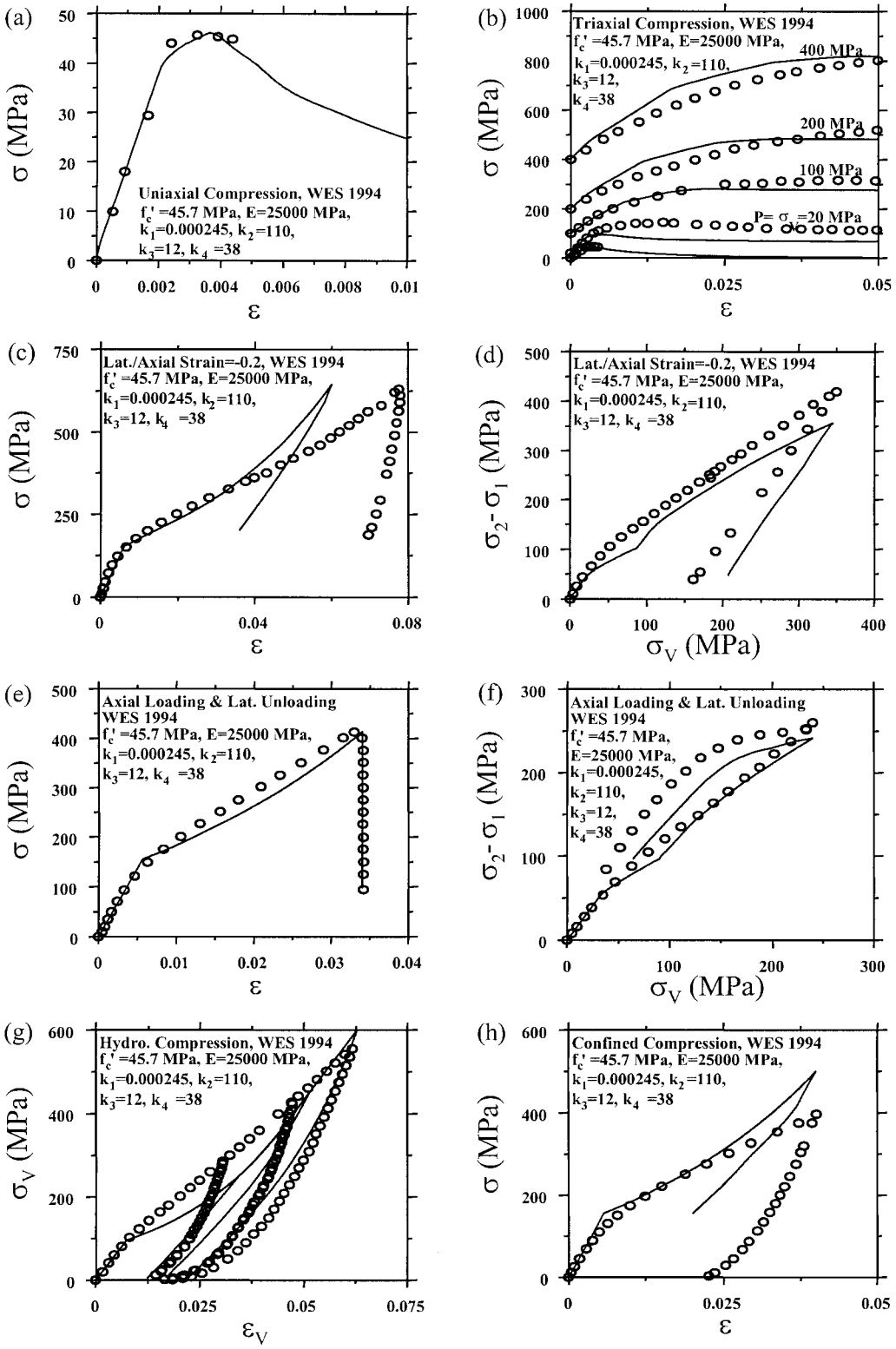

FIG. 2. Test Data Obtained at WES (Bažant et al. 1996b) Compared to Optimized Fits by Model M4

The confined compression test data by Bažant et al. (1986) are simulated in Fig. 1(f). The agreement between the test data and the model is good, even in the unloading regime.

The hydrostatic compression test data by Green and Swanson (1973) and the corresponding response of the model are pictured in Fig. 1(g). Again, the model is shown to simulate material response under hydrostatic loading very accurately. Note the similar nature of the data and the fits in Figs. 1(f and g). These fits are governed by the compressive volumetric boundary and verify that the exponential curve used for this boundary works well.

Fig. 2(g) shows the hydrostatic compression test data from WES and the simulated response. These data could be better fit by using a bilinear curve for the compression volumetric boundary, but the exponential boundary that fits most other data best, for example, those in Figs. 1(f and g), has been retained to preserve the generality of the model. Still, the fit is close enough in the loading regime. In the unloading regime,

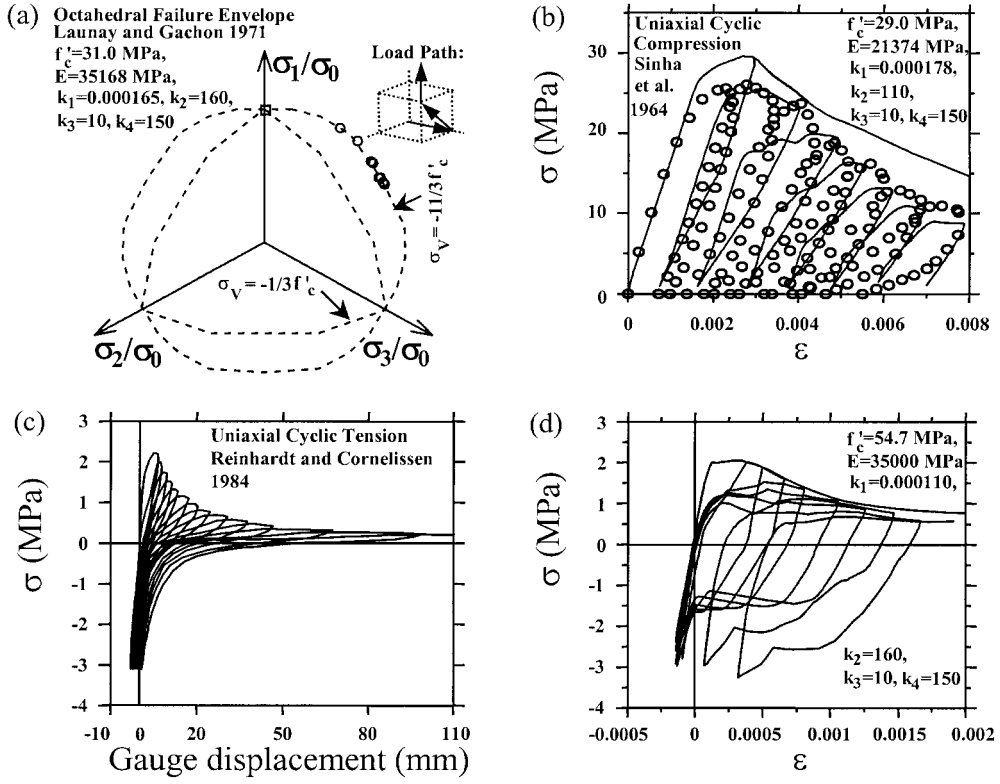

FIG. 3. Further Basic Test Data from Literature Compared to Optimized Fits by Model M4

the damage indicated by the test data is also described reasonably well.

The confined compression tests at WES are simulated in Fig. 2(h). The unloading branches do not agree well with the WES data, but this is entirely caused by deciding to fit with only four free material parameters many unusual types of tests with nonproportional loading made on the same concrete, and enforcing the same values of all the fixed parameters for all the concretes. If a few fixed parameters were changed to additional free parameters, all the WES tests could be matched closely, including the unloading branches. However, this would be a complication for the user. The goal of this study is to produce, not a set of particular models applicable only to certain concretes, but one general model applicable to any concrete. With such a goal, one must accept some misfits, such as those in Fig. 2(c).

Ideally, the strain field in a test specimen should remain homogeneous, except for statistical fluctuations due to heterogeneity of the microstructure. In postpeak strain softening, this is impossible to ensure. This gives rise to the difficult questions of strain localization and size effect, which can at best be resolved only approximately. Neither 3D nor 2D analysis is feasible, not only because of its difficulty but also because strain redistributions have not been measured. Therefore, one must become contented with a 1D model for longitudinal localization, as described in Sec. 13.1 of Bažant and Cedolin (1991, Part II).

The only study in which postpeak localization and size effect have been reported is that of van Mier (1984, 1986). Previous analysis in Bažant and Cedolin (1991, Part II, Sec. 13.2) showed that van Mier's data agree with (and thus validate) the simple 1D (series coupling) model of longitudinal localization, which was then applied in Bažant et al. (1996a) for delocalization of test data. Van Mier's compression test data used in Fig. 1(a), however, need not be delocalized because they pertain to the shortest of his specimens, having a size that can be regarded as the representative volume of the material. For the various bi- and triaxial tests considered here, delocalization is not only impossible, for lack of data, but it is probably also not too important because the triaxial restraints in such tests must have hindered localizations.

Thus it seems that the only data that need delocalization are the uniaxial tensile test data of Petersson (1981). Display of the actual measurements reported is preferred, and so comparisons with the model M4 require that the model predictions be localized. Therefore, the reverse of the delocalization procedure formulated in Bažant et al. (1996a) was applied to the predictions of model M4, which led to the curves in Fig. 1(h). As seen, good predictions are achieved again (the same set of parameter values is, of course, used for both data sets in the figure). As in the case of the uniaxial (unconfined) compression, the postpeak slope can be easily adjusted to fit any similar test data.

Fig. 3(b) shows the cyclic test data of Sinha et al. (1964) in uniaxial compression. Applying the rate-independent model M4 as described here, the hysteretic loops in Sinha et al.'s tests were too narrow. Therefore, the simulations plotted in the figures include the viscoelastic rate effect (short-time creep) described in a subsequent study (Bažant et al. 2000b). However, the effect of the fracturing rate described in that study is not considered because it does not affect the width of the hysteretic loops.

Finally, Reinhardt and Cornelissen's (1984) data for cyclic uniaxial tension-compression and the corresponding response from the model M4 are shown in Figs. 3(c and d). The experimental data were obtained using notched specimens, and the measured variable was the relative displacement between two points near the opposite sides of the crack. This displacement should be proportional to the average tensile strain in the fracture process zone predicted by M4, although the proportionality factor would be hard to determine from model M4 (it would require nonlocal finite-element analysis). Therefore, the two figures are presented side by side for comparison. This comparison of course cannot verify the prediction of strain

magnitudes, but it does prove that the shapes of hysteretic loops predicted by M4 are approximately correct.

TANGENTIAL STIFFNESS MATRIX AND LOCALIZATION LIMITER

To allow implicit solutions and checks for bifurcations, one needs the tangential stiffness matrix. On the structural level, this may be done as follows: All the nodal displacements are fixed as 0 except one, which is set equal to a number δ of very small magnitude, positive or negative, depending on the direction of loading. The nodal forces are then calculated with the finite-element program based on model M4. Dividing them by δ yields one row of the tangential stiffness matrix of the structure. This is then repeated for each nodal displacement, and thus all the rows of the stiffness matrix are obtained.

The tangential stiffness matrix of the material may be generated similarly, setting as 0 the increments of all strain tensor components except one, which is set equal to δ. Solving the stress increments with the explicit microplane model yields one row of the tangential stiffness matrix. Alternatively, the tangential stiffness matrix can also be calculated from the tangents of the microplane stress-strain relations (Bažant and Prat 1988a, Part 1).

Because concrete exhibits strain softening, it is necessary to limit spurious localization on the structural level. This problem has been extensively researched over the last two decades, and various approaches that have been developed, such as the integral or gradient-type nonlocal concepts or the crack-band concept, can be applied. The method for the nonlocal integral-type approach was described in detail in Bažant et al. (1996b, Part 1) [also Bažant and Ožbolt (1990, Part 1) and Ožbolt and Bažant (1996)].

Examples of structural analysis are left for a subsequent paper in this issue (Bažant et al. 2000c).

SUMMARY AND CONCLUSIONS FROM PARTS 1 AND 2

1. The present new version M4 of the microplane model for concrete features several conceptual improvements:
   a. A work-conjugate volumetric deviatoric split, which is not a strictly requisite feature but greatly improves the physical interpretation of stress components.
   b. Additional horizontal boundaries (yield limits) for the normal and deviatoric microplane stress components, which make it possible to control the curvature at peaks of stress-strain curves. These boundaries also make it possible to simulate plastic behavior (they could even produce a plateau of any length on the macroscopic stress-strain curve).
   c. Nonlinear frictional yield surface with plastic asymptote for the microplanes.
   d. A simpler, more effective fitting procedure, with sequential identification of material parameters, which retains the previously introduced simple scaling properties and makes possible an immediate adjustment of the model to a given strength limit and strain at peak stress.
   e. A method to control the steepness and tail length of postpeak softening.
   f. Damage modeling with a reduction of unloading stiffness and tensile crack closing boundary.
2. The model predictions agree with the basic experimental data distinctly better than either of the previous versions of the microplane model for concrete or other nonlinear constitutive models. The model is not difficult to calibrate for a given particular set of data. Although many parameters are involved, all except four need not be adjusted for given particular data since they can be taken with the same values as specified here for all types of concretes. The four free parameters can be calibrated for the given particular data set by a simple sequential procedure. The algorithm for implementing the model has been clearly formulated and is ready for use as a material subroutine in computer programs for nonlinear structural analysis with step-by-step loading.

APPENDIX I. DRIVER OF MATERIAL SUBROUTINE

The algorithm for the driver of the material subroutine outlined in the paper is given below. It must be noted that [*Prescribed Boundary Conditions*] below refers to a vector where prescribed stress or strain increments are combined together, and not to traction and displacement at the boundary of a finite body.

1. Given the vectors [*Prescribed Boundary Conditions*], [*Previous Stress*], [*Previous Strain*], [*Stress*], and [*Strain*]
2. Calculate the current [*Stiffness Matrix*]
3. Set the vectors [*Satisfied Boundary Conditions*], [*Stress Increment*], [*Strain Increment*], [*Accumulated Stresses*], and [*Accumulated Strains*] equal to zero; then iterate over the following:
4. a. Set [*Stress*] = [*Prescribed Boundary Conditions*] − [*Satisfied Boundary Conditions*]
   b. Copy [*Stiffness Matrix*] as [*Copied Stiffness Matrix*]
   c. Arrange [*Stress*] and [*Copied Stiffness Matrix*] depending on [*Prescribed Boundary Conditions*], then solve the matrix equation [*Copied Stiffness Matrix*] [*Unknown Strain*] = [*Stress*] for the vector [*Unknown Strain*]
   d. Compute [*Unknown Stress*] corresponding to [*Unknown Strain*] according to the linear elastic constitutive law
   e. Accumulate computed [*Unknown Stresses*] and [*Unknown Strain*] as [*Accumulated Stress*] and [*Accumulated Strain*] and pass [*Accumulated Strain*] to the material subroutine, the algorithm for which is outlined in the paper
   f. Assign [*Stress Increment*] = [*Final Stress*] − [*Previous Stress*]
   g. Assign [*Satisfied Boundary Conditions*] = [*Stress Increment*] if the stress increments are prescribed at a given degree of freedom, or [*Satisfied Boundary Conditions*] = [*Prescribed Boundary Conditions*] if the strain increments are prescribed at that degree of freedom (the last assignment implies that, when all the degrees of freedom contain solely the strain increments, then the model becomes explicit and there are no iterations taking place)
   h. Continue to iterate unless the given tolerance is satisfied (the tolerance may be specified as the length of the difference of [*Prescribed Boundary Conditions*] and [*Satisfied Boundary Conditions*], excluding from this difference vector the components for which the strains have been prescribed)
5. Assign [*Strain*] = [*Previous Strain*] + [*Accumulated Strain*], [*Stress*] = [*Previous Stress*] + [*Accumulated Stress*] and update [*Previous Stress*] = [*Stress*] and [*Previous Strain*] = [*Strain*]
6. Output [*Stress*] and [*Strain*], go to the next loading step

ACKNOWLEDGMENTS

Grateful appreciation is due to the U.S. Army Engineer Waterways Experiment Station (WES), Vicksburg, Mississippi, for funding the work of Z. P. Bažant under contract number DACA39-94-C-0025 with Northwestern University. F. C. Caner wishes to thank the National Science

Foundation for funding his doctoral research under grant CMS-9713944 to Northwestern University, which enabled him to devise and improve many of the stress-strain boundaries, formulate and program the algorithm, develop the sequential fitting procedure, and calibrate the model by test data.

APPENDIX II. REFERENCES

Aschl, H., Linse, D., and Stöckl, S. (1976). ''Strength and stress-strain behavior of concrete under multiaxial compression and tension loading.'' *Tech. Rep.*, Technische Universität München, Germany.

Balmer, G. G. (1949). ''Shearing strength of concrete under high triaxial stress—Computation of Mohr's envelope as a curve.'' *Struct. Res. Lab. Rep. No. SP-23*, U.S. Department of the Interior and Bureau of Reclamation, Denver.

Bažant, Z. P., et al. (2000a). ''Large-strain generalization of microplane model for concrete and application.'' *J. Engrg. Mech.*, ASCE, 126(9), 971–980.

Bažant, Z. P., Bishop, F. C., and Chang, T.-P. (1986). ''Confined compression tests of cement paste and concrete up to 300 ksi.'' *J. Am. Concrete Inst.*, 33(4), 553–560.

Bažant, Z. P., Caner, F. C., Carol, I., Adley, M. D., and Akers, S. A. (2000c). ''Microplane model M4 for concrete: I: Formulation with work-conjugate deviatoric stress.'' *J. Engrg. Mech.*, ASCE, 126(9), 944–953.

Bažant, Z. P., Caner, F. C., Adley, M. A., and Akers, S. A. (2000b). ''Fracturing rate effect and creep in microplane model for dynamics.'' *J. Engrg. Mech.*, ASCE, 126(9), 962–970.

Bažant, Z. P., and Cedolin, L. (1991). *Stability of structures: Elastic, inelastic, fracture and damage theories*, Oxford University Press, New York.

Bažant, Z. P., and Ožbolt, J. (1990). ''Nonlocal microplane model for fracture, damage, and size effect in structures.'' *J. Engrg. Mech.*, ASCE, 116(11), 2485–2505.

Bažant, Z. P., and Prat, P. C. (1988a). ''Microplane model for brittle plastic material. I: Theory.'' *J. Engrg. Mech.*, ASCE, 114(10), 1672–1688.

Bažant, Z. P., and Prat, P. C. (1988b). ''Microplane model for brittle plastic material. II: Verification.'' *J. Engrg. Mech.*, ASCE, 114(10), 1689–1699.

Bažant, Z. P., Xiang, Y., Adley, M. D., Prat, P. C., and Akers, S. A. (1996a). ''Microplane model for concrete. II: Data delocalization and verification.'' *J. Engrg. Mech.*, ASCE, 122(3), 255–262.

Bažant, Z. P., Xiang, Y., and Prat, P. C. (1996b). ''Microplane model for concrete. I: Stress-strain boundaries and finite strain.'' *J. Engrg. Mech.*, ASCE, 122(3), 245–254.

Bresler, B., and Pister, K. S. (1958). ''Strength of concrete under combined stresses.'' *J. Am. Concrete Inst.*, 551(9), 321–345.

Cofer, W. F., and Kohut, S. W. (1994). ''A general nonlocal microplane concrete material model for dynamic finite element analysis.'' *Comp. and Struct.*, 53(1), 189–199.

Goode, C. D., and Helmy, M. A. (1967). ''The strength of concrete under combined shear and direct stress.'' *Mag. of Concrete Res.*, 1959, 105–112.

Green, S. J., and Swanson, S. R. (1973). ''Static constitutive relations for concrete.'' *Rep. No. AFWL-TR-72-2*, Air Force Weapons Lab., Kirtland Air Force Base, Albuquerque, N.M.

Kupfer, H., Hilsdorf, H. K., and Rüsch, H. (1969). ''Behavior of concrete under biaxial stresses.'' *J. Am. Concrete Inst.*, 66, 656–666.

Launay, P., and Gachon, H. (1971). ''Strain and ultimate strength of concrete under triaxial stress.'' *Proc., 1st Int. Conf. on Struct. Mech. in Reactor Technol.* (*SMiRT1*), T. Jaeger, ed., Commission of European Communities, Brussels.

Ožbolt, J., and Bažant, Z. P. (1996). ''Numerical smeared fracture analysis: Nonlocal microcrack interaction approach.'' *Int. J. Numer. Methods in Engrg.*, Chichester, U.K., 39, 635–661.

Petersson, P. E. (1981). ''Crack growth and development of fracture zones in plain concrete and similar materials.'' *Rep. No. TVBM 1006*, Lund Institute of Technology, Lund, Sweden.

Reinhardt, H. W., and Cornelissen, H. A. W. (1984). ''Post-peak cyclic behavior of concrete in uniaxial tensile and alternating tensile and compressive loading.'' *Cement and Concrete Res.*, 14(2), 263–270.

Sinha, B. P., Gerstle, K. H., and Tulin, L. G. (1964). ''Stress-strain relations for concrete under cyclic loading.'' *J. Am. Concrete Inst.*, 62(2), 195–210.

van Mier, J. G. M. (1984). ''Strain-softening of concrete under multiaxial loading conditions.'' PhD dissertation, De Technische Hogeschool Eindhoven, The Netherlands.

van Mier, J. G. M. (1986). ''Multiaxial strain-softening of concrete. I: Fracture; II: Load histories.'' *Mat. and Struct.*, 111(19), 179–200.